View metadata, citation and similar papers at core.ac.uk

brought to you by CORE

provided by Online Research Database In Technology

DTU Library

An Experimental Demonstration of Rate- Adaptation Using Shaped Polar Codes for Flexible Optical Networks

Iqbal, Shajeel; Porto da Silva, Edson; Yankov, Metodi Plamenov; Oxenløwe, Leif Katsuo; Forchhammer, Søren

Published in:
Journal of Lightwave Technology

Link to article, DOI:
10.1109/JLT.2019.2915916

Publication date:
2019

Document Version
Peer reviewed version

Link back to DTU Orbit

Citation (APA):
Iqbal, S., Porto da Silva, E., Yankov, M. P., Oxenløwe, L. K., & Forchhammer, S. (2019). An Experimental Demonstration of Rate- Adaptation Using Shaped Polar Codes for Flexible Optical Networks. Journal of Lightwave Technology, 37(13), 3357 - 3364. https://doi.org/10.1109/JLT.2019.2915916

General rights
Copyright and moral rights for the publications made accessible in the public portal are retained by the authors and/or other copyright owners and it is a condition of accessing publications that users recognise and abide by the legal requirements associated with these rights.

- Users may download and print one copy of any publication from the public portal for the purpose of private study or research.
- You may not further distribute the material or use it for any profit-making activity or commercial gain
- You may freely distribute the URL identifying the publication in the public portal

If you believe that this document breaches copyright please contact us providing details, and we will remove access to the work immediately and investigate your claim.

This article has been accepted for publication in a future issue of this journal, but has not been fully edited. Content may change prior to final publication. Citation information: DOI 10.1109/JLT.2019.2915916, Journal of Lightwave Technology

An Experimental Demonstration of Rate-Adaptation Using Shaped Polar Codes for Flexible Optical Networks

Shajeel Iqbal, Edson P. da Silva *Senior Member, IEEE, Member, OSA,* Metodi P. Yankov *Member, IEEE,* Leif K. Oxenløwe *Member, IEEE, Fellow, OSA,* and Søren Forchhammer *Member, IEEE*

***Abstract*—In this paper, we propose a polar-coded transmission system with adjustable data rate for coherent optical transmission employing quadrature amplitude modulation (QAM). The proposed system is based on a many-to-one constellation shaping method for achieving a range of data rates with arbitrarily small rate steps. An implicitly punctured polar-coded modulation system is then designed by combining polar coded bit-interleaved coded modulation system (BICM) with many-to-one labellings. The scheme is experimentally evaluated in a wavelength division multiplexed (WDM) system with five carriers modulated at 16 GBaud with polarization multiplexed (PM) 256QAM. Data rates ranging from 121 Gbps to 182 Gbps per carrier are experimentally demonstrated and the system can be directly extended to achieve higher data rates. Synchronization and equalization of PM-256QAM received symbols is performed with a pilot rate of 5%. The experimental results show 1.2 dB of shaping gain over the conventionally punctured polar codes in the optical back-to-back scenario. The maximum transmission system reach is increased by 200 km to 400 km w.r.t the conventionally punctured polar codes. It is shown that the rate adaptation does not require a change of modulation format and/or underlying forward error-correction (FEC) code. Finally, the performance of all 5 WDM channels is validated for the optimal input power.**

***Index Terms*—Polar codes, Experimental demonstration, probabilistic shaping, wavelength division multiplexing (WDM), Rate-adaptation**

I. Introduction

MODERN optical communication systems utilize all the available resources to meet the tremendous growth in the demand for high data rates. These systems are based on coherent receiver technologies exploiting both polarizations, advanced modulation formats and available spectral efficiency (SE) [1]−[3]. Advanced modulation formats combined with FEC codes, called coded modulation (CM) systems, have become a vital part of optical networks [4]. The CM systems must adapt their SE to the available signal-to-noise ratio (SNR), to support varying data rates. Varying data rates or SEs can be achieved by using different modulation formats [2] and one or two FEC engines with different overheads [5]. However, the flexibility is still limited and there are implementation challenges with such schemes.

The CM systems with varying data rates can be realized with low-density parity-check (LDPC) codes [6]−[10] as they are capable of achieving near-optimal performance with acceptable complexity of encoder and decoder. However, for standard and irregular LDPC codes, the encoder/decoder must be designed for each desired SE [5], [10], which requires additional hardware. A rate-adaptive CM system for LDPC codes was designed in [6] using a probabilistic amplitude shaping (PAS), which concatenates a distribution matcher (DM) [11] with a systematic FEC encoder requiring an additional shaping encoder and shaping decoder, thus increasing complexity at the transmitter and receiver. Most modern communication systems employ packet based transmission at higher layers and at the high levels the whole packet is discarded if any bit is in error. The standard DM de-matching [11], like all other non-linear DMs, leads to (bit-) error-propagation [12]. For a given post-FEC frame error rate (FER), this bit error-propagation will not affect FER at the lower layer and at most have minor influence on packet error-rates at higher protocol layers. However the post-DM receiver output BER may potentially be higher than the target post-FEC BER [12, Sec. VII]. This should be considered when using BER as figure of merit as often done in optical communication. Considering both FER and BER, BER could be used to assess secondary effects or in special cases be the interesting or specified figure of merit.

Polar codes [13] are known to asymptotically achieve the capacity of any discrete memory-less symmetric channel with low complexity encoding and decoding algorithms outperforming e.g., WiMAX LDPC codes [14]. It is also proven that the successive cancellation (SC) decoder for polar codes does not display an error floor [15], as compared to LDPC codes which display an error floor if they are not carefully designed for each SE [9]. Hardware based polar decoders of short code lengths are already under investigation for 5G [16], [17] due to their ability to achieve Gbps throughput at less area, power and energy consumption than the WiMAX LDPC codes [16]. As a potential candidate for future lightwave systems, the

Parts of this paper have been presentated at the 44th European Conference on Optical Communications (ECOC), Roma, Italy, Sep. 2018. [28]

This work was supported by the DNRF Research Centre of Excellence, SPOC, ref. DNRF123.

E. P. da Silva is with the Department of Electrical Engineering of the Federal University of Campina Grande (UFCG), Paraíba, Brazil (email: edson.silva@dee.ufcg.edu.br). He was also supported by National Council for Scientific and Technological Development (CNPq), Brazil, grant 432214/2018-6.

M. P. Yankov is with Fingerprint Cards A/S, 2730 Herlev, Denmark and with Department of Photonics Engineering, Technical University of Denmark, Kongens Lyngby 2800, Denmark (email: meya@fotonik.dtu.dk)

S. Iqbal, L. K. Oxenløwe and S. Forchhammer are with Department of Photonics Engineering, Technical University of Denmark, Kongens Lyngby 2800, Denmark (email: shaip@fotonik.dtu.dk, lkox@fotonik.dtu.dk, sofo@fotonik.dtu.dk)

0733-8724 (c) 2019 IEEE. Personal use is permitted, but republication/redistribution requires IEEE permission. See http://www.ieee.org/publications_standards/publications/rights/index.html for more information.

This article has been accepted for publication in a future issue of this journal, but has not been fully edited. Content may change prior to final publication. Citation information: DOI 10.1109/JLT.2019.2915916, Journal of Lightwave Technology

performance of SC polar decoder was compared with state-of-the-art spatially coupled LDPC codes in [18]. However, polar codes perform best with list decoding [14]. Therefore, polar codes can be further investigated for future flexible optical communication networks using list decoding.

Originally, polar codes were proposed for the code lengths which were powers of two, while the code dimension (the number of data bits) can be arbitrary. The common techniques to obtain a polar code of any rate and length are based on puncturing [19]−[22] at the cost of increased BER. These methods were proposed for 5G systems and could also be applied to optical systems incorporating wireless technologies such as hybrid fiber-wireless systems [23]. Another potential use for short punctured polar codes can be similar to the concatenated FEC scheme composed by an outer staircase code and a soft-decision Hamming code specified in [24] targeting 400G data center interconnect. Hamming codes can be replaced by short polar codes in high-end optical communication for even better performance.

Multi-level polar codes combined with PAS and DM have been studied in [25] for short packets. This combination increases the latency and complexity at the transmitter and receiver due to the use of DM and multi-level decoding. Another probabilistic shaping method for polar codes was proposed in [26]. The scheme in [26] uses a list decoder to generate the shaping bits at the transmitter for each codeword. Therefore, this scheme also increases the latency and complexity at the transmitter.

In this paper, we propose a system which provides a high degree of rate-adaptivity combining puncturing and shaping. It uses a many-to-one constellation shaping method achieving a gain which recovers the puncturing loss of polar codes. The proposed many-to-one mapping is an instance of many-to-one probabilistic shaping as originally proposed by Gallager in [27, p. 208]. The system design provides a highly flexible rate-adaptive system in terms of transmission rate based on one mother code, and thus without increasing the system and implementation complexity. We extend our first simulated system in [28] and experimentally investigate a flexible polar-coded modulation scheme that increases the transmission distance w.r.t the conventionally punctured polar codes for a range of data rates with fine granularity in step size. We find that the gains predicted by additive white Gaussian noise (AWGN) channel simulations can be achieved for wavelength division multiplexing (WDM) scenarios, where both intra- and inter-channel non-linearities are present.

The rest of the paper is organized as follows: In Section II, we describe the preliminaries of polar codes including their encoding and decoding algorithm. In Section III, we discuss the puncturing for polar codes and show how the puncturing can lead to performance degradation. We then propose to use a many-to-one constellation shaping method to recover the puncturing loss of polar codes. Sections IV, V and VI are the main contributions of this paper where we apply the proposed system to an optical transmission system. In Section IV, we present the experimental setup for the fiber transmission followed by back-to-back experiments and transmission experiments in Sections V and VI, respectively. Section VII concludes this paper.

II. Preliminaries of Polar Codes

A polar code of length N, dimension K and rate $R = K/N$ is defined by its generator matrix $G_N = G_2^{\otimes n}$, where $n = \log_2(N)$, $\otimes$ denotes the Kronecker product,

$$G_2 = \begin{pmatrix} 1 & 0 \\ 1 & 1 \end{pmatrix} \tag{1}$$

and by a *frozen set* $I \subseteq \{1, 2, ..., N\}$. The *frozen set* can be determined by evaluating the bit reliabilities of the underlying channel. The bit reliabilities can be estimated by various methods [29]−[33]. In this work, we used the method proposed in [31] for computing the bit reliabilities. The bit positions with least reliabilities are assigned to the *frozen set* I, while the data is sent over the highly reliable bit positions.

A. Encoding of Polar Codes

Let $u_1^N = [u_1, u_2, ..., u_N]$ be the vector containing K information bits and $N - K$ frozen bits, then the codeword vector $x_1^N = [x_1, x_2, ..., x_N]$ for a polar code can be obtained as follows:

$$x_1^N = u_1^N B_N G_N \tag{2}$$

where B_N is the $N \times N$ bit-reversal permutation matrix [13]. The polar coding maps the information bits u_1^K to the K most reliable bit positions as defined by the *frozen bits* set I . The remaining $N - K$ bit positions are set to zero. The codeword x_1^N can then be obtained by (2). Note that the rate R of the polar code can be easily changed by selecting/deselecting the frozen bits.

B. Decoding of Polar Codes

Arikan proposed the successive cancellation (SC) decoder for polar codes in [13]. Let $y_1^N = [y_1, y_2, ..., y_N]$ denote the channel output vector. The SC decoder sequentially decodes the bits from index 1 to index N. For each index i an estimate on bit $\hat{u}_i$ is made, if $i \in I$ then $\hat{u}_i$ is set to its frozen value i.e., $\hat{u}_i = 0$ in our case. On the other hand, if $i \in K$ then $\hat{u}_i$ is set to the most likely value given by the channel output vector y_1^N and by the previous estimates $[\hat{u}_1, \hat{u}_2, ..., \hat{u}_{i-1}]$. The dependence of estimated value on previous estimates in the SC decoder leads to propagation of error in the SC tree, once an error occurred in the decoding. Due to this the SC decoder has poor performance.

A successive cancellation list decoder (SCL) has been proposed [14] to improve the performance of polar codes greatly. In SCL decoding hard decision on the estimated bits $\hat{u}_i$ is avoided by considering both possible values of $\hat{u}_i$ i.e., $\hat{u}_i = 0$ and $\hat{u}_i = 1$. Thus whenever a decision has to be made on $\hat{u}_i$ both paths with $\hat{u}_i = 0$ and $\hat{u}_i = 1$ are followed by the decoder, resulting in two decodable paths or lists. This process is continued and it could lead to an exponential increase in the number of decodable paths. Therefore the number of paths is limited to a fixed value L. Whenever the number of paths reaches $2L$, the paths with lowest reliabilities are deleted and the L best paths are kept for further decoding. When the

0733-8724 (c) 2019 IEEE. Personal use is permitted, but republication/redistribution requires IEEE permission. See http://www.ieee.org/publications_standards/publications/rights/index.html for more information.

This article has been accepted for publication in a future issue of this journal, but has not been fully edited. Content may change prior to final publication. Citation information: DOI 10.1109/JLT.2019.2915916, Journal of Lightwave Technology

decoding is terminated, the path with the highest reliability is chosen as the output of the decoder. A cyclic redundancy check (CRC) can be appended to the input bits to further improve the performance of the decoder. This decoder is referred to as CRC-aided (CA)-SCL decoder. In the case of CA-SCL decoding the path which passes the CRC is chosen as the output of the decoder instead of simply the most probable one. The CA-SCL decoder has been shown to perform better than WiMAX LDPC codes [14].

III. Puncturing of Polar codes

Puncturing is the method of obtaining a code of length $N_l = N - P$ from a code of length N. The puncturing vector P is defined as:

$$P_1^l = [P_1, P_2, ..., P_l], \tag{3}$$

where l is its length and $(P_1, P_2, ..., P_l)$ indicates the indices of the codeword bits to be punctured. Thus l codeword bits are not sent during the transmission which increases the rate of the code. At the decoder these bits are treated as erased bits i.e., their log likelihood values are set to zero. Puncturing can degrade the performance of a channel code, therefore care must be taken in choosing the puncturing vector P.

A. Explicit Puncturing of Polar Codes

Originally, polar codes were proposed to be constructed for a power of 2, i.e. $N = 2^n$, where $(n = 1, 2, 3, ...)$. A polar code of any length can be obtained by puncturing. Conventionally, a punctured polar code (N_l, K_l) can be obtained from a base polar code (N, K) with $N_l = N - P$ and $K_l = K$ by puncturing. The punctured vector in the case of a polar code is defined as:

$$P_1^l = B_{N_l}[P_1, P_2, ..., P_l], \tag{4}$$

where B_{N_l} denotes the bit-reversal permutation of the vector $P_1^l = [P_1, P_2, ..., P_l]$ i.e., the first l bits of codeword x_1^N chosen in bit-reversal order are punctured. This method of puncturing is called as *quasi-uniform puncturing* and was proposed in [20]. Since some of the codeword bits are explicitly selected to not be transmitted, we refer to this type of puncturing *explicit puncturing of polar codes* (EPPCs). The log-likelihood ratios (LLRs) of these bits seen by the CA-SCL decoder are zero. The performance degradation due to explicit puncturing is exemplified in Fig. 1.

In Fig. 1 we consider the BER performance of 256 QAM for various code lengths i.e., $N = 8192, 6554$, and 4096 with input data rate $\eta = 5$ bits/symbol over the AWGN channel. The code length $N_l = 6554$ is a punctured code from the base code of length $N = 8192$ with $l = 1638$. It can be seen from Fig. 1, that the punctured code $(6554, 4096)$ performs about 1 dB worse than its base code $(8192, 5120)$ for the same η. This penalty originates from the puncturing. The interesting comparison to see is between the base polar code $(4096, 2560)$ and the punctured code $(6554, 4096)$. We observe that a longer polar code of length $N_l = 6554$ with higher coding gain performs 0.6 dB worse than a shorter polar code of length $N = 4096$, due to puncturing. In the next section, we propose a solution to this problem, where a polar code will be able

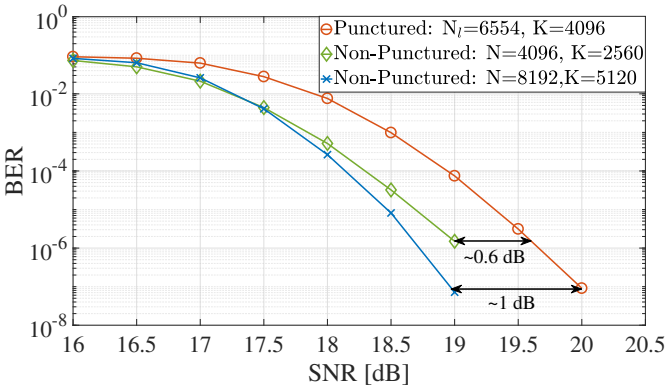

Fig. 1. **AWGN Simulation**: BER performance comparison of punctured and non-punctured polar codes with $\eta = 5$, list-size 32 and 32-bit CRC. The number of punctured bits is $l = 1638$ for the punctured polar code.

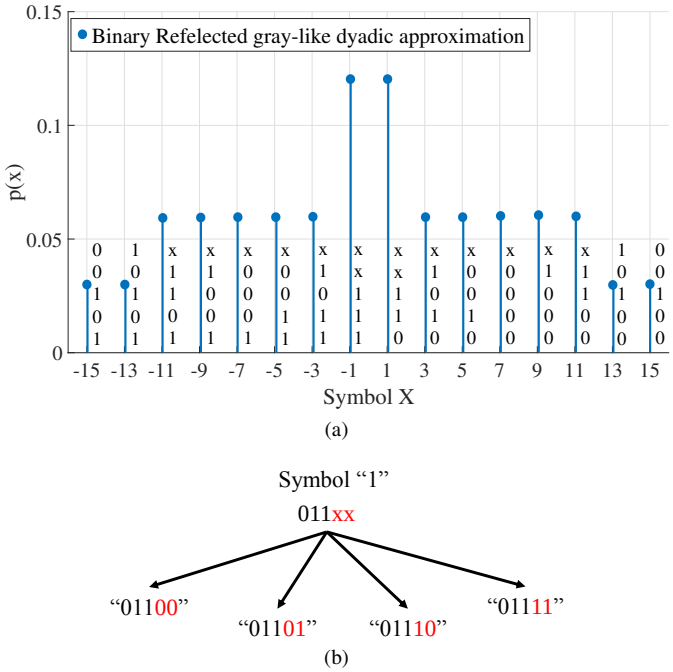

Fig. 2. (a) Dyadic distributions and many-to-one mappings obtained using the algorithm in [38]. (b) Many-to-one mappings for the symbol '1'.

to recover from the loss of puncturing using shaping without incurring any additional overhead.

B. Implicit Puncturing of Polar Codes

Implicit puncturing of polar codes in this work is based on the many-to-one constellation shaping method [34]. Constellation shaping is the method of obtaining non-uniform distribution of the data from the uniformly distributed data. Thus with shaping, the distribution of the modulated symbols can be changed.

Various methods have been proposed by the researchers to shape the modulated symbols e.g., shell mapping [35], trellis shaping [36], PAS [6] and iterative polar modulation [37]. One method of obtaining non-uniform distribution is through dyadic approximations. A dyadic distribution has the form $p_X(X = x_i) = 2^{-d_i}$, where d_i is an integer. In order to ensure

0733-8724 (c) 2019 IEEE. Personal use is permitted, but republication/redistribution requires IEEE permission. See http://www.ieee.org/publications_standards/publications/rights/index.html for more information.

This article has been accepted for publication in a future issue of this journal, but has not been fully edited. Content may change prior to final publication. Citation information: DOI 10.1109/JLT.2019.2915916, Journal of Lightwave Technology

that the resultant constellations form a binary-reflected gray code, the algorithm from [38] is followed. In the optical fiber scenarios considered in this work the following distribution for 16-ary pulse amplitude modulation (PAM) was found to be the optimal choice of the available families of dyadic distributions:

$$p(x_i = \pm 13, \pm 15) = 1/2^5$$
$$p(x_i = \pm 3, \pm 5, \pm 7, \pm 9, \pm 11) = 1/2^4$$
$$p(x_i = \pm 1) = 1/2^3, \quad (5)$$

as defined in [38] and shown in Fig. 2(a). This distribution is found by maximizing the achievable information rate (AIR) at the optimal launch power, under the constraint that we map integer bits at symbol level. The QAM symbols are obtained by taking the product of marginal distributions in each I and Q.

In many-to-one mappings multiple bit sequences are mapped to the same symbol from the constellation. Due to this, the bit label length is greater than $\log_2(M)$ as opposed to standard QAM where the bit label length is always equal to $\log_2(M)$, where M is the constellation alphabet size. This creates ambiguities in some bit positions as shown in Fig. 2 by 'x'. From Fig. 2(b), it can be seen that the symbol '1' with bit label '011xx' has two ambiguous bits marked as 'x'. Thus the bit sequences which are mapped to symbol '1' are '01100', '01101', '01110', and '01111'. Many-to-one maximum a-posteriori probability de-mapping will result in low certainty at the ambiguous bits, and they will be treated as punctured by the FEC decoder. Since puncturing is data dependent and thus unknown by the decoder, we refer to this type of puncturing as *implicit puncturing of polar codes* (IPPCs). Implicit puncturing of polar codes has also been studied in [39], where the use of multiple encoders and decoders leads to many short codes degrading the performance of the code as well as increasing the latency and complexity of the system. Many-to-one mappings were also evaluated for LDPC codes with 16-QAM [10] achieving 7% increase in transmission reach over the uniform mappings. The LDPC code designed in [10] is irregular and designed to match the mapping function i.e., the LDPC code should be changed when the mapping and SNR are changed, implying that the system is not rate-adaptive.

We adapted the rate adaptive turbo-coded modulation system from [38] for polar codes as shown in Fig. 3. The binary data u_1^N containing the information bits are fed to the systematic polar encoder. The data and parity bits are then interleaved separately using a pseudo-random interleaver. The many-to-one mapper maps the coded bits to QAM symbols while implicitly puncturing some of the parity bits according to the many-to-one mapper. At the receiver, the signal is demodulated and the data are deinterleaved. The parity bits are de-punctured and then sent for CA-SCL decoding together with data bits.

We simulated the transmitter and receiver from Fig. 3 over an AWGN channel. We studied the BER performance of 256 QAM with non-punctured polar codes (NPPCs), EPPC and IPPC schemes. The simulated input data rates are from 4 to 6 with a step size of 1. All the evaluated codes are decoded

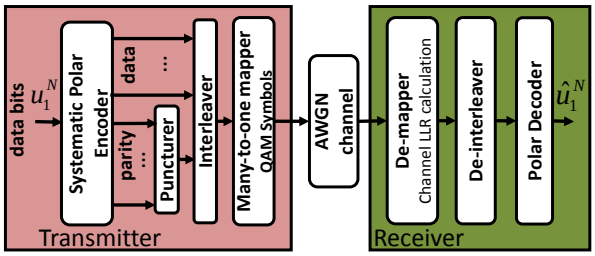

Fig. 3. Polar-coded BICM transmitter and receiver with many-to-one mapper.

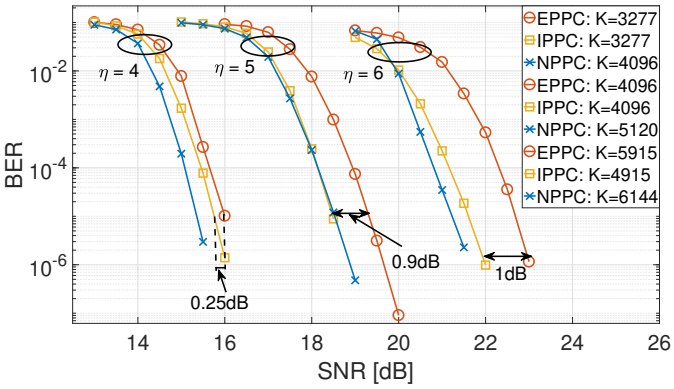

Fig. 4. **AWGN Simulation**: BER performance of NPPC, EPPC and IPPC schemes with 256-QAM. The code length for EPPC scheme is $N_l = 6554$ with $l = 1638$ while the code length for rest of the cases is $N = 8192$.

using CA-SCL decoding with 32-bit CRC and list size 32. The code length considered here is $N = 8192$ and for EPPC the code length is $N_l = 6554$ with $l = 1638$ punctured bits. The total number of transmitted symbols in case of EPPC and IPPC schemes are same i.e. 820 symbols for $N = 8192$. It can be seen from Fig. 4 that IPPC scheme provides a gain of 0.9 dB and 1 dB over the EPPC scheme for $\eta = 5$ and $\eta = 6$, respectively. The gain provided by IPPC scheme over EPPC scheme for $\eta = 4$ is limited to 0.25 dB. This is due to the small code rate where the number of parity bits is larger than the data bits, implying powerful coding which in turn helps the decoder to recover the puncturing loss. At the simulated BER, the rate adaptive code could be used as inner code and combined with a longer hard decision outer code.

The complexity of QAM demappers scales linearly with $m = \log_2(M)$ [40]. For many-to-one demappers more bits per symbol needs to be demapped which slightly increases the complexity of the demapper [41]. Compared to the other probabilistic schemes for polar codes such as in [25], [26], the IPPC scheme does not require an additional shaping encoder or shaping decoder. Moreover, with the IPPC scheme very fine granularity in rate step can be achieved by changing the number of parity bits in polar code, which can be realized without any additional hardware complexity and latency at the receiver.

In the next sections we present an experimental study of the polar-coded transmitter and receiver from Fig. 3 for an optical transmission system.

0733-8724 (c) 2019 IEEE. Personal use is permitted, but republication/redistribution requires IEEE permission. See http://www.ieee.org/publications_standards/publications/rights/index.html for more information.

This article has been accepted for publication in a future issue of this journal, but has not been fully edited. Content may change prior to final publication. Citation information: DOI 10.1109/JLT.2019.2915916, Journal of Lightwave Technology

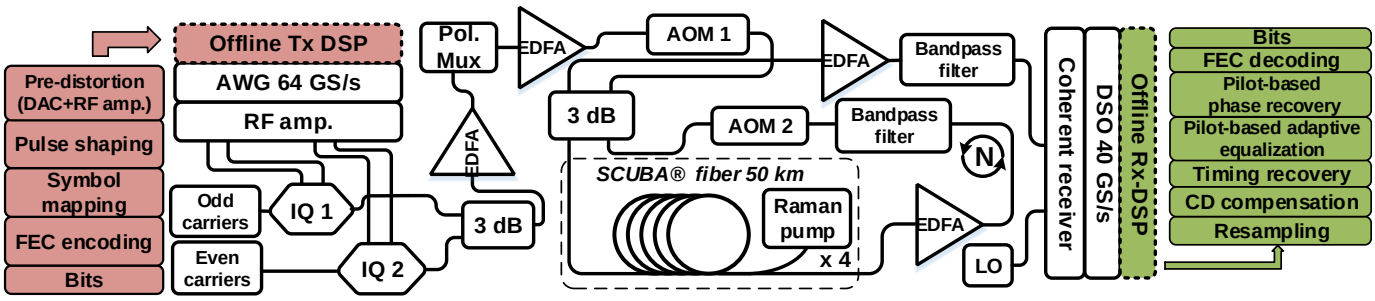

Fig. 5. Experimental setup of the WDM experiment including a detailed block diagram of the offline DSP utilized at the transmitter and at the receiver.

IV. Experimental Setup

The experimental setup is shown in Fig. 5. The WDM system is composed of five carriers modulated at 16 GBd and disposed in a grid spacing of 25 GHz. All optical carriers in the experiment are external cavity lasers with 10 kHz linewidth. The transmitted symbols are generated by encoding pseudo random bit sequences. The encoded bits are interleaved and mapped to 256 QAM symbols. A 5% overhead of 16 QAM pilot symbols is added to assist the adaptive equalization and the carrier phase recovery at the receiver. The symbols are pulse shaped with a root-raised cosine (RRC) filter with 401 taps and a roll-off factor of 0.05. A linear pre-emphasis is applied to pre-compensate for the joint frequency response of transmitter and receiver. Two decorrelated sequences containing 60 frames of FEC encoded data are loaded in the arbitrary waveform generator (AWG). After amplification, each baseband signal drives one of two in-phase/quadrature (IQ) modulators. After combining even and odd modulated carriers with a coupler, the signal is amplified with an Erbium-doped fiber amplifier (EDFA) to compensate for the power losses of the optical modulators. The WDM system is sent to a delay-and-combine polarization multiplexing emulation stage ($\approx$ 953 symbol periods of decorrelation). In the last stage of the transmitter, the polarization multiplexed signal is amplified by a booster EDFA.

In back-to-back configuration, the maximum effective received SNR of the central WDM channel saturates at 20.5 dB. The WDM channels propagate in a recirculating loop composed of four 50 km spans of submarine ultra-large area fiber (OFS SCUBA fiber), with all propagation losses compensated by distributed Raman amplification (backward pumping configuration). An EDFA is added after the fiber spans to compensate for the insertion losses of couplers and switches. After performing coherent detection, the signal is sampled at 40 GS/s with a real-time oscilloscope (20 GHz of analog bandwidth). In the offline digital signal processing (DSP), the acquired signal passes through a front-end compensation stage, resampling, chromatic dispersion (CD) compensation, low-pass filtering, timing recovery, $T_s/2$-fractionally spaced pilot-based adaptive equalization (85 taps), and pilot-based carrier frequency and phase recovery with a moving average phase estimator. Finally, the estimated symbols are sent to the FEC decoder.

V. Back-to-back transmission results

We performed experimental characterization of the three schemes, i.e. NPPC, EPPC and IPPC. Input data rates from 4 to 6 with a step size of 0.5 were tested for each scheme. We refer to the experimental points on the plots with no errors as error-free. We experimentally evaluated a total of 120 frames i.e. 9.8×10^5 bits for each channel. The details of all the schemes are summarized in the Table I.

The performance for $\eta = 5$ bits/symbol is shown in Fig. 6. In Fig. 6(a), we plotted the estimated received SNR versus the measured optical SNR (OSNR). The green line indicates the theoretical SNR and was calculated according to [1, Eq. 34]. It can be seen from Fig. 6(a), that implementation penalty at low OSNR is 3 dB, and thereafter gradually increases to 4.5 dB and even further for higher OSNR. The implementation penalty is due to the non-ideal hardware and DSP implementation.

The AIR is estimated from the mutual information (MI) using the Gaussian auxiliary channel principle [42] are compared in Fig. 6(b) for all three schemes. At $\eta = 5$ bits/symbol, the shaping gain w.r.t to uniform 256 QAM and punctured 256 QAM is about 1.5 - 2 dB. The IPPC scheme here operates at around 4.2 dB gap to the Shannon capacity at $\eta = 5$ bits/symbol. We see that the implementation penalty is about 2.8 dB and 4.2 dB at 18 dB and 24 dB OSNR, respectively. This implementation penalty also includes the residual phase noise and sub-optimal estimation of the auxiliary channel parameters..

We also show the BER performance versus OSNR in Fig. 6(c). It can be seen that the EPPC scheme suffers up to $\approx$1.5 dB loss for fixed BER compared to the NPPC scheme. However, this loss can be recovered by up to 1.2 dB from the

TABLE I
Summary of NPPC, EPPC and IPPC schemes

Scheme	η [bits/symbol], Data rate [Gbps/channel]				
	4, 121.6	**4.5, 136.8**	**5, 152**	**5.5, 167.2**	**6, 182.4**
NPPC	N=8192 K=4096	N=8192 K=4608	N=8192 K=5120	N=8192 K=5632	N=8192 K=6144
EPPC	N_l=6554 K=3277 l=1638	N_l=6554 K=3686 l=1638	N_l=6554 K=4096 l=1638	N_l=6554 K=4506 l=1638	N_l=6554 K=4915 l=1638
IPPC	N=8192 K=3277	N=8192 K=3686	N=8192 K=4096	N=8192 K=4506	N=8192 K=4915

0733-8724 (c) 2019 IEEE. Personal use is permitted, but republication/redistribution requires IEEE permission. See http://www.ieee.org/publications_standards/publications/rights/index.html for more information.

This article has been accepted for publication in a future issue of this journal, but has not been fully edited. Content may change prior to final publication. Citation information: DOI 10.1109/JLT.2019.2915916, Journal of Lightwave Technology

IPPC scheme combined with shaping at the same transmission rate. The gain is similar to the AWGN simulation results shown in Fig. 4.

VI. Transmission Experiment Results

In order to further investigate the system performance over a transmission link, we apply all the three schemes to the transmission experiment over a recirculating loop explained in Section IV.

A. Central Channel

The considered channel parameters for this case are given in Table II. The achieved error-free data rate and the AIR are shown in Fig. 7, at the respective optimal input power, as a function of the link distance for the central channel. The distances from 200 km to 4000 km are studied for all three schemes with η varying from 4 to 6 bits/symbol. We selected an input data rate and keep on increasing the distance until error-free transmission was not possible with that data rate. This has been done with all considered schemes from Table I. It can be seen from Fig. 7, that the IPPC scheme with shaping recovers the puncturing loss and provides an increase of 200 km of distance for $\eta = 4.5$ to $\eta = 6$ compared to the EPPC scheme at the same data rate. It can also be observed that the error-free distance of IPPC scheme for $\eta = 4$ is increased by 400 km over the EPPC scheme. We see that the NPPC and IPPC schemes are able to operate at around 0.65 bits/symbol gap to the AIR, which is mainly attributed to the rather short code lengths considered here i.e., $N = 8192$. Longer codes were not considered due to the long processing time on a personal computer. It is important to note here that the achieved error-free data rates of IPPC and NPPC are similar, and our IPPC scheme provides ≈0.2 bits/symbol steady gain over the EPPC scheme due to shaping.

TABLE II
System Parameters for WDM Transmission

Symbol rate	16 GBaud
Pulse shape	square-root raised cosine
Roll-off factor	0.05
Channel Spacing	25 GHz
Number of Channels	5
Input data rates	4, 4.5, 5, 5.5 and 6 bits/symbol
Pilot overhead	5%

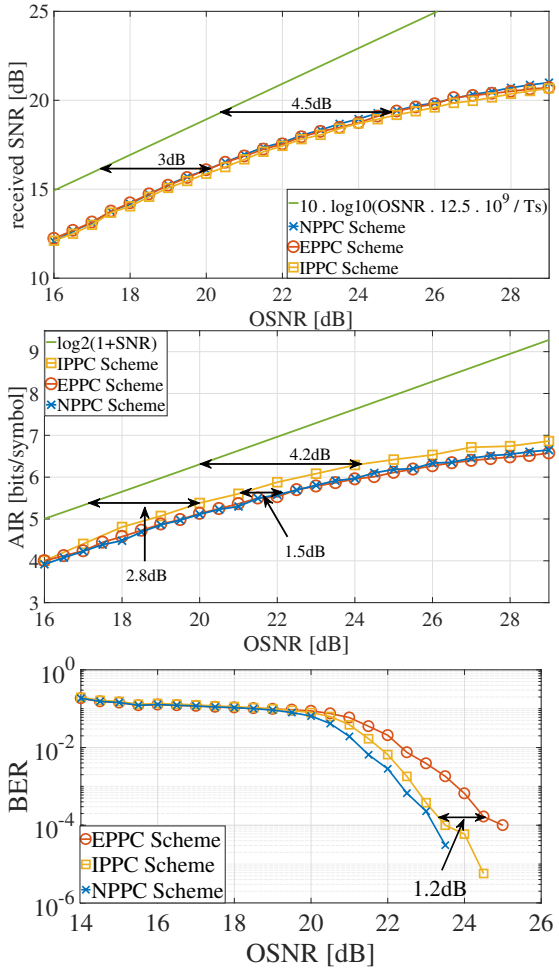

Fig. 6. **Back-to-back**: Performance in optical back-to-back for NPPC, EPPC and IPPC schemes. (a) Estimated received SNR. (b) Estimated AIR. (c) Calculated BER.

B. WDM Measurements for all Channels

Finally, we performed WDM measurements for all 5 channels at the optimal input power. The WDM measurements are performed by tuning the local oscillator and the transmitter laser to the desired channel on the frequency grid. The input power of each channel is optimized, so that all the channels have the same received power for all the schemes. The average AIR for all 5 channels is shown in Fig. 8. The error bars in Fig. 8 are estimated by taking the difference between the average AIR for all 5 channels and the maximum/minimum AIR among all WDM channels. Similarly, the error bars for distance are measured by taking the difference between the error-free transmission distance of the central channel and the channel which has the longest error-free distance. We show the curves for EPPC and IPPC schemes from Table I. First we notice from Fig. 8, that the average performance is similar to the central channel shown in Fig. 7. Thus, some channels potentially achieve longer error-free transmission distance compared to the other channels. In general, the distances at which Channel 1 and 5 achieve error-free performance are somewhat longer than the other 3 channels. For example, the error-free distances are increased by 200 km for Channels 1 and 5 compared to Channels 2, 3 and 4. This is due to the fact, that Channels 1 and 5 only have 1 neighbour and thus suffer less linear and non-linear interference. The difference in performance of all WDM channels also come from the tilted noise spectrum of the amplification and a performance difference between the optical IQ modulators. It should also be noted here that each loop turn adds 200 km of distance and thus we have limited resolution in terms of distance. It maybe noted that the single rate-adaptive code effectively can be adapted to a wide range of AIRs and thereby distances.

0733-8724 (c) 2019 IEEE. Personal use is permitted, but republication/redistribution requires IEEE permission. See http://www.ieee.org/publications_standards/publications/rights/index.html for more information.

This article has been accepted for publication in a future issue of this journal, but has not been fully edited. Content may change prior to final publication. Citation information: DOI 10.1109/JLT.2019.2915916, Journal of Lightwave Technology

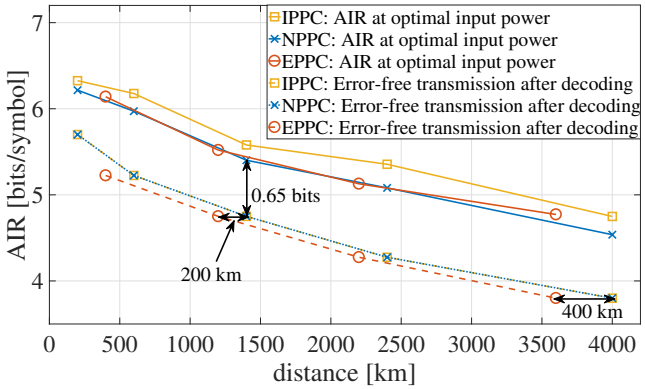

Fig. 7. **WDM Transmission for central channel**: AIRs at the optimal input power for the studied systems (solid lines) and error-free operating points (dashed lines) after CA-SCL decoding for code length $N = 8192$.

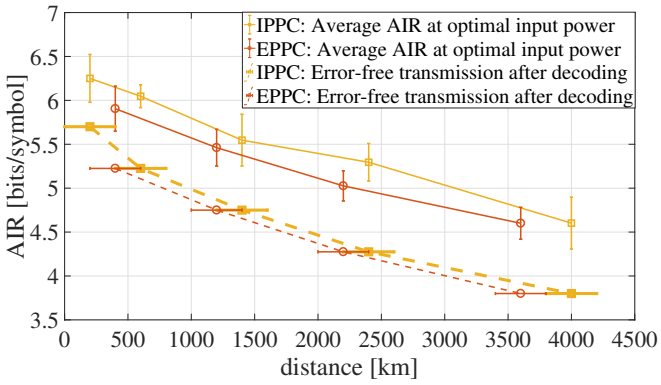

Fig. 8. **WDM Transmission for all channels**: AIRs at the optimal input power for EPPC and IPPC schemes (solid lines) and error-free operating points (dashed lines) after CA-SCL decoding for code length $N = 8192$.

VII. Conclusion

In this paper, we applied a 256QAM many-to-one probabilistic shaping in order to enable rate-adaptive punctured polar-coded modulation. The system relies on the combination of polar codes with many-to-one mapping function providing a flexible optical transmission system operating at adjustable data rate with fine granularity. Rate-adaptivity is achieved using implicit puncturing that allows one to select any operating point without changing the modulation format, bandwidth, baud rate and/or underlying FEC code and without performance penalty. Thus, the proposed system does not require additional hardware for rate-adaptivity. Higher modulation formats and baud rates can also be realized by the direct extension of the proposed system.

The method was experimentally demonstrated on a 5 WDM dually polarized coherent transmission system at 16 GBaud/channel. We demonstrated that the puncturing loss of polar codes can be recovered by implicit puncturing of polar codes combined with shaping providing an increase of around 0.2 bits/symbol, or alternatively the maximum transmission reach is increased by 200 km for short distances (<2500 km) and by 400 km for long distances (>3500 km), w.r.t the conventionally punctured polar codes. Robust performance was achieved using one code over a range of 200 km to 4000 km.

References

[1] R. -J. Essiambre, G. Kramer, P. J. Winzer, G. J. Foschini, and B. Goebel, "Capacity Limits of Optical Fiber Networks," *J. Lightw. Technol.*, vol. 28, no. 4, pp. 662-701, Feb. 2010.

[2] E. Agrell and M. Karlsson, "Power-efficient modulation formats in coherent transmission systems," *J. Lightw. Technol.*, vol. 27, no. 22, pp. 5115-5126, Nov. 2009.

[3] B. P. Smith and F. R. Kschischang, "Future prospects for FEC in fiber-optic communications," *IEEE J. Select Topics Quantuum Electron.*, vol. 16, no. 5, pp. 1245-1257, Sep. 2010.

[4] ITU-T G.975.1, "Forward error correction for high bit-rate DWDM submarine systems," Feb. 2004.

[5] *Digital Video Broadcasting (DVB); Second Generation Framing Structure, Channel Coding and Modulation Systems for Broadcasting, Interactive Services, News Gathering and Other Broadband Satellite Applications; Part 2: DVB-S2 Extensions (DVB-S2X)*, Eur. Telecommun. Standards Inst., (ETSI) Std. EN 302 307-2, Rev. 1.1.1, 2014.

[6] G. Böcherer, P. Schulte, and F. Steiner, "Bandwidth Efficient and Rate-Matched Low-Density Parity-Check Coded Modulation," *IEEE Trans. Commun.*, vol. 63, no. 12, pp. 4651-4665, Dec. 2015.

[7] F. Buchali, F. Steiner, G. Böcherer, L. Schmalen, P. Schulte, and W. Idler, "Rate Adaptation and Reach Increase by Probabilistically Shaped 64-QAM: An Experimental Demonstration," *J. Lightw. Technol.*, vol. 34, no. 7, pp. 1599-1609 Apr. 2016.

[8] L. Beygi, E. Agrell, J. M. Kahn, and M. Karlsson, "Rate-Adaptive Coded Modulation for Fiber-Optic Communications," *J. Lightw. Technol.*, vol. 32, no. 2, pp. 333-343, Jan. 2014.

[9] G. Tzimpragos, C. Kachris, I. B. Djordjevic, M. Cvijetic, D. Soudris, and I. Tomkos, "A Survey on FEC Codes for 100 G and Beyond Optical Networks," *IEEE Comm. Sur. Tut.*, vol. 18, no. 1, pp. 209-221, Oct. 2014.

[10] C. Pan and F. R. Kschischang, "Probabilistic 16-QAM Shaping in WDM systems," *J. Lightw. Technol.*, vol. 34, no. 18, pp. 4285-4292, July. 2016.

[11] P. Schulte and G. Böcherer, "Constant composition distribution matching," *IEEE Trans. Inf. Theory*, vol. 62, no. 1, pp. 430-434, Nov. 2016.

[12] T. Yoshida, M. Karlsson, and E. Agrell, "Hierarchical Distribution Matching for Probabilistically Shaped Coded Modulation," *J. Lightw. Technol.*, [Early Access]. doi: 10.1109/JLT.2019.2895065

[13] E. Arikan, "Channel Polarization: A Method for Constructing Capacity-Achieving Codes for Symmetric Binary-Input Memoryless Channels," *IEEE Trans. Inf. Theory*, vol. 55, no. 7, pp. 3051-3073, Jun. 2009.

[14] I. Tal and A. Vardy, "List Decoding of Polar Codes," *IEEE Trans. on Inf. Theory*, vol. 61, no. 5, pp. 2213-2226 May 2015.

[15] M. Mondelli, S. H. Hassani, and R. L. Urbanke, "Unified Scaling of Polar Codes: Error Exponent, Scaling Exponent, Moderate Deviations, and Error Floors," *IEEE Trans. Inf. Theory*, vol. 62, no. 12, pp. 6698-6712 Dec. 2016.

[16] F. Ercan, C. Condo, S. A. Hashemi, and W. J. Gross, "On error-correction performance and implementation of polar code list decoders for 5G," *Annual Allerton Conf. Comm., Control, and Computing*, pp. 443-449 Oct. 2017.

[17] V. Bioglio, C. Condo, and I. Land, "Design of Polar Codes in 5G New Radio," available online (https://arxiv.org/abs/1804.04389).

[18] L. Schmalen, V. Aref, J. Cho, D. Suikat, D. Rosener, and A. Leven, " Spatially Coupled Soft-Decision Error Correction for Future Lightwave Systems," *J. Lightw. Technol.*, vol. 33, no. 5, pp. 1109-1116, Mar. 2015.

[19] R. Wang and R. Liu, " A novel puncturing scheme for polar codes," *IEEE Comm. Letters*, vol. 18, no. 12, pp. 208-2084, Dec. 2014.

[20] K. Niu, K. Chen, and J. -R. Lin, "Beyond turbo codes: Rate-compatible punctured polar codes," *IEEE Intl. Conf. Commun.(ICC)*, pp. 3423-3427, Jun. 2013.

[21] D. -M. Shin, S. -C. Lim, and K. Yang, "Design of length-compatible polar codes based on the reduction of polarizing matrices," *IEEE Tran. on Commun.*, vol. 61, no. 7, pp. 2593-2599, July 2013.

[22] V. Bioglio, F. Gabry, and I. Land, "Low-Complexity Puncturing and Shortening of Polar Codes," *IEEE Wireless Communications and Networking Conference Workshops (WCNCW)*, pp. 1-6, May 2017.

[23] N. Ghazisaidi, M. Maier, and C. M. Assi, "Fiber-wireless (FiWi) access networks: A survey," *IEEE Commun. Mag.*, vol. 47, no. 2, pp. 160-167, Feb. 2009.

[24] B. Smith, I. Lyubomirsky, and S. Bhoja, "Leveraging 400G ZR FEC Technology," *IEEE 802.3 Beyond 10km Optical PHYs*

0733-8724 (c) 2019 IEEE. Personal use is permitted, but republication/redistribution requires IEEE permission. See http://www.ieee.org/publications_standards/publications/rights/index.html for more information.

This article has been accepted for publication in a future issue of this journal, but has not been fully edited. Content may change prior to final publication. Citation information: DOI 10.1109/JLT.2019.2915916, Journal of Lightwave Technology

Study Group, Orlando, FL, USA, Nov. 2017. [Online]. Available: http://www.ieee802.org/3/B10K/public/17_11/lyubomirsky_b10k_01_1117.pdf

[25] T. Prinz, P. Yuan, G. Böcherer, F. Steiner, O. Iscan, R. Bohnke, and W. Xu, "Polar coded probabilistic amplitude shaping for short packets," *IEEE 18th Intl. Workshop on Sig. Proc. Adv. in Wireless Commun. (SPAWC)*, Sapporo, pp. 1-5, 2017.

[26] O. İşcan and W. Xu, "Polar codes with integrated probabilistic shaping for 5G new radio," *arXiv preprint*, 2018. [Online]. Available. https://arxiv.org/abs/1808.09360.

[27] R. G. Gallager, *Information Theory and Reliable Communication.* John Wiley and Sons, Inc., 1968.

[28] S. Iqbal, M. P. Yankov, and S. Forchhammer, "Rate-Adaptive Polar-Coded Constellation Shaping for Flexible Optical Networks," *IEEE European Conf. on Optical Comm. (ECOC)*, pp. 1-3, Sep. 2018.

[29] I. Tal and A. Vardy, "How to construct polar codes," *IEEE Transactions on Information Theory*, vol. 59, no. 10, pp. 6562-6582, Oct. 2013.

[30] P. Trifonov, "Efficient design and decoding of polar codes," *IEEE Transactions on Communications*, vol. 60, no. 11, pp. 1-7, Nov. 2012.

[31] R. Mori and T. Tanaka, "Performance of polar codes with the construction using density evolution," *IEEE Comm. Lett.*, vol. 13, no. 7, pp. 519-521, Jul. 2009.

[32] P. Yuan, T. Prinz, and G. Böcherer, "Polar codes construction for list decoding," *arXiv preprint*, 2017. [Online]. Available. https://arxiv.org/abs/1707.09753.

[33] G. Böcherer, T. Prinz, P. Yuan, and F. Steiner, "Efficient polar code construction for higher-order modulation," *IEEE Wireless Commun. Net. Conf. Workshops (WCNCW)*, San Francisco, CA, 2017, pp. 1-6.

[34] D. Raphaeli and A. Gurevitz, "Constellation shaping for pragmatic turbo-coded modulation with high spectral efficiency," *IEEE Transactions on Communications*, vol. 52, no. 3, pp. 341-345, Mar. 2004.

[35] A. K. Khandani and P. Kabal, "Shaping multidimensional signal spaces. I. optimum shaping, shell mapping," *IEEE Trans. Inf. Theory*, vol. 39, no. 6, pp. 1799-1808, Nov. 1993.

[36] G. D. Forney, "Trellis Shaping," *IEEE Trans. Inf. Theory*, vol. 38, no. 2, pp. 281-300, Mar. 1992.

[37] I. B. Djordjevic, H. G. Batshon, L. Xu, and T. Wang, "Coded Polarization-Multiplexed Iterative Polar Modulation(PM-IPM) for Beyond 400 Gb/s Serial Optical Transmission," *Optical Fiber Communication Conference (OFC)*, May. 2010, paper OMK2.

[38] M. P. Yankov, S. Forchhammer, K. J. Larsen, and L. P. B. Christensen, "Rate-adaptive constellation shaping for near-capacity achieving turbo coded BICM, *IEEE Intl. Conf. Comm.*, pp. 2112-2117, Aug.2014.

[39] D. Zhou, K. Niu, and C. Dong, "Constellation shaping for bit-interleaved polar coded-modulation," *IEEE Intl. Symp. PIMRC*, pp. 1-5, Dec. 2016.

[40] Q. Wang, Q. Xie, Z. Wang, C. Sheng, and L. Hanzo, "A Universal low-complexity symbol-to-bit soft demapper," *IEEE Trnas. Veh. Technol.*, vol. 63, no. 1, pp. 119-130, Jan. 2014.

[41] M. P. Yankov, F. Da Ros, E. P. da Silva, S. Forchhammer, K. J. Larsen, L. K. Oxenlwe, M. Galili, and D. Zibar, "Constellation Shaping for WDM Systems Using 256QAM/1024QAM With Probabilistic Optimization", J. Lightw. Technol., vol. 34, no. 22, pp. 5146-5156, Nov. 2016.

[42] G. Kaplan and S. Shamai(Shitz), "Information rates and Error exponents of compound channels with application to antipodal signaling in a fading environment," *AEU*, vol. 47, no. 4, pp. 228-239, 1991.

0733-8724 (c) 2019 IEEE. Personal use is permitted, but republication/redistribution requires IEEE permission. See http://www.ieee.org/publications_standards/publications/rights/index.html for more information.